Atmos. Chem. Phys. Discuss., 15, 28037–28068, 2015
www.atmos-chem-phys-discuss.net/15/28037/2015/
doi:10.5194/acpd-15-28037-2015

Atmospheric Chemistry and Physics Discussions

A Lagrangian description on the troposphere-to-stratosphere transport changes associated with the stratospheric water drop around the year 2000

F. Hasebe[1,2] **and T. Noguchi**[2,a]

[1]Faculty of Environmental Earth Science, Hokkaido University, Sapporo, Japan
[2]Graduate School of Environmental Science, Hokkaido University, Sapporo, Japan
[a]now at: Human Asset Management and Corporate Affairs Unit, FUJITSU FSAS INC., Kawasaki, Japan

Received: 10 August 2015 – Accepted: 17 September 2015 – Published: 19 October 2015

Correspondence to: F. Hasebe (f-hasebe@ees.hokudai.ac.jp)

Published by Copernicus Publications on behalf of the European Geosciences Union.

Abstract

Stratospheric water vapor is known to have decreased suddenly at around the year 2000 to 2001 after a prolonged increase through the 1980s and 1990s. This stepwise change is studied by examining the entry value of water to the stratosphere ($[H_2O]_e$) and some Lagrangian diagnostics of dehydration taking place in the Tropical Tropopause Layer (TTL). The analysis is made using the backward kinematic trajectories initialized every ~ 10 days since January 1997 till December 2002 on 400 K potential temperature surface in the tropics. The $[H_2O]_e$ is estimated by the ensemble mean value of the water saturation mixing ratio (SMR) at the Lagrangian cold point (LCP) where SMR takes minimum (SMR_{min}) in the TTL before reaching the 400 K surface. The drop in $[H_2O]_e$ is identified to have occurred in September 2000. The horizontal projection of September trajectories, tightly trapped by anticyclonic circulation around Tibetan high, shows eastward expansion since the year 2000. Associated changes are measured by three-dimensional bins, each having the dimension of 10° longitude by 10° latitude within the TTL. The probability distribution of LCPs shows appreciable change exhibiting a composite pattern of two components: (i) the dipole structure consisting of the decrease over the Bay of Bengal and Malay Peninsula and the increase over the northern subtropical western Pacific and (ii) the decrease over the equatorial western Pacific and the increase over the central Pacific almost symmetric with respect to the equator. The SMR_{min} shows general decrease in the tropics with some enhancement in the central Pacific. The expectation values, defined by the multiple of the probability of LCP events and the ensemble mean values of SMR_{min}, are calculated on each bin for both periods prior and posterior to the drop. These values are the spatial projection of $[H_2O]_e$ on individual bin. The results indicate that the drop is brought about by the decrease of water transport borne by the air parcels having experienced the LCP over the Bay of Bengal and the western tropical Pacific. The former is related to the eastward expansion of the anticyclonic circulation around the weakened Tibetan high, while the latter will be linked to the eastward expansion of western tropi-

ACPD
15, 28037–28068, 2015

cal warm water to the central Pacific. This oceanic surface forcing may be responsible also for the modulation of dehydration efficiency in the successive northern winter. The drop in September 2000 and the sustained low values thereafter of $[H_2O]_e$ are thus interpreted as being driven by the changes in thermal forcing from the continental and oceanic bottom boundaries.

1 Introduction

Stratospheric water vapor (SWV) observed by balloon-borne hygrometers exhibits gradual increase in the 1980s and 1990s (Oltmans and Hofmann, 1995; Oltmans et al., 2000) followed by a stepwise drop at around the year 2000 (Scherer et al., 2008; Fujiwara et al., 2010). Since SWV has a positive radiative forcing as a greenhouse gas (Shindell, 2001), its possible increase during the two decades could have caused enhanced surface warming by about 30 % as compared to that without taking this increase into account, while the subsequent drop could have slowed down the surface warming by about 25 % from about 0.14 to 0.10 °C per decade (Solomon et al., 2010). The cause and mechanism of this stepwise change have been fluently discussed (e.g., Randel et al., 2006; Rosenlof and Reid, 2008; Bönisch et al., 2011; Fueglistaler, 2012; Fueglistaler et al., 2014; Dessler et al., 2014). While constructing a reliable long-term SWV record is still a challenge (Hegglin et al., 2014), the understanding of a possible stepwise change in SWV is required in assessing possible modulation of the Brewer–Dobson circulation under global warming.

The variation of SWV is driven dynamically by the troposphere-to-stratosphere transport of water and chemically by the oxidation of methane. The dynamical control is mostly associated with the efficiency of dehydration functioning on the air mass advected in the TTL (Holton and Gettelman, 2001; Hatsushika and Yamazaki, 2003). The reproduction of SWV variations by using the Lagrangian temperature history along the trajectories (e.g., Fueglistaler et al., 2005; Dessler et al., 2014) has proven quite effective, even though the quantitative estimation of the water amount entering the

ACPD
15, 28037–28068, 2015

stratosphere requires detailed consideration dealing with aerosols and ice particles (ice nucleation and sublimation processes, supersaturation, and deposition and precipitation of ice particles) as well as the minute description of meteorological conditions (subgrid-scale variabilities, intrusion of deep convection into advected air parcels, and irreversible mixing due to breaking waves along with the ambiguity in the analysis field).

Here, we discuss the cause of the stepwise drop in SWV by making the analysis of the entry mixing ratio of water to the stratosphere ($[H_2O]_e$) with the aid of some Lagrangian diagnostics of TTL dehydration such as the preferred advection pathways in the TTL, the location in which water saturation mixing ratio (SMR) takes minimum along each trajectory (Lagrangian cold point; LCP) together with its occasional value (SMR_{min}) before entering the stratosphere (Sect. 3). The backward kinematic trajectories initialized on 400 K potential temperature surface in the tropics, similar to those of Fueglistaler et al. (2005), are used. The calculations cover the period from January 1997 to December 2002. The statistical features of the LCP and SMR_{min} are analyzed for the 90 day trajectories in which the air parcels experienced LCP in the TTL (Sect. 2). The analysis is focused on the examination of the entry value of water to the stratosphere, meaning that any contribution from the recirculation within the stratosphere (ST) and the sideway entry of water to ST without taking the LCP in the TTL are intentionally left out of the scope. Detailed examinations on the driving mechanism itself are left for future studies. However, it will reveal the direct cause that may have led to the SWV drop in Lagrangian framework. This approach has the advantages over Eulerian description because the drop in SWV does not necessarily mean TTL cooling conveniently described in Eulerian framework. For example, it might simply reflect the change in the proportion of air parcels that have passed the coldest region in the TTL. Conversely, any extreme cooling does not necessarily result in enhanced dehydration as long as the air parcels do not experience LCP event in that region. We will try to describe a hypothetical story on the cause of the stepwise drop of SWV through the discussion of the results in Sect. 4. Conclusions are placed in Sect. 5.

ACPD
15, 28037–28068, 2015

2 Method of analysis

2.1 Trajectory calculations

The method of estimating $[H_2O]_e$ in the present study is similar to that of Fueglistaler et al. (2005). $[H_2O]_e$ at time t is estimated as the ensemble mean value of SMR_{min} along 90 day backward kinematic trajectories initialized at t. The trajectory calculations are started from uniformly distributed gridpoints (every 5.0° longitude by 1.5° latitude) within 30° N and S from the equator on 400 K potential temperature surface, which results in 2952 initialization points in total for a single calculation. The calculations are started from the 5th, 15th, and 25th of every month during the period since January 1997 till December 2002 relying on the European Centre For Medium-Range Weather Forecasts ERA Interim dataset (Dee et al., 2011). All meteorological variables on the 60-layer model levels have been converted to those on pressure levels keeping the horizontal resolution of 0.75° by 0.75° longitude–latitude gridpoints prior to calculations.

2.2 Selection of trajectories relevant to TTL dehydration

The meridional projections of the backward trajectories extracted from those initialized on 15 January 1999 are shown in Fig. 1. The top and bottom diagrams are the same except that pressure (top) and potential temperature (bottom) are taken as the ordinate. The asterisks in red indicate the location of the LCP while those in green are the termination point of trajectory calculations (90 days before initialization at the longest). In case the backward extension of the trajectories hit the surface of the earth, the calculations are terminated at that point, and those portions of the trajectories immediately before the surface collision are used for the analysis. The migration of air parcels depicted in the trajectories is roughly categorized into three major branches: quasi-isentropic advection in the TTL and the lower stratosphere (LS), vertical displacement in the troposphere due to diabatic motion resolvable in grid-scale velocity field, and quasi-isentropic migration in the troposphere. We can see many air parcels are traced

ACPD
15, 28037–28068, 2015

back to the troposphere representing the tropical troposphere-to-stratosphere transport (TST), while some portion of the trajectories remain in the LS and/or reach the tropical 400 K surface by taking the sideways without making excursions in the TTL. All non-TST trajectories are removed from the following analysis to focus our discussion on the modulation of $[H_2O]_e$. For the sake of clarity, the TST particles in the present study are defined as a subset of those particles traceable down to 340 K having recorded LCP in the TTL. For the application of this LCP condition to our trajectories, we introduce the Lagrangian definition of the TTL to assure internal consistency of the analysis.

The motion of air parcels ascending in the tropical troposphere is characterized by rapid convective up-lift that accompanies latitudinal migration associated with the seasonal displacement of the Inter-Tropical Convergence Zone. Up in the TTL, on the other hand, the diabatic ascent is driven by radiative heating, in which the seasonal migration with respect to latitude is much smaller than that in the troposphere because the dynamical field generated by the thermal forcing at the bottom boundary retains relatively high symmetry with respect to the equator. By translating these features into the characteristics of trajectories, we derive a definition of the TTL in a Lagrangian fashion.

Figure 2 on the top illustrates the vertical distribution of the proportion of trajectories categorized on a daily basis as "fast" ascending air parcels. The required rate for the fast ascent is set to more than 0.2 K in potential temperature within 1 time step (30 min), that is, the condition for θ K isentrope is met if the air parcel crosses θ K surface from below $\theta - 0.1$ K to above $\theta + 0.1$ K in 30 min. We can see that the proportion of the fast diabatic ascent thus defined takes maximum at around 340 K in the troposphere and minimum at around 355 K. The proportion of such "fast" air parcels reduces above the level of main outflow and rapidly decays toward the level of zero net radiative heating in the TTL. Above this level, the air parcels are diabatically lifted up by radiative heating and further pumped-up by dissipating planetary waves in the midlatitude stratosphere (Holton et al., 1995). The alternation of the primary forcing that drives diabatic ascent is also seen from the bottom panel of Fig. 2, which shows the seasonal migration of the latitudinal position of the trajectories traceable to down below 340 K averaged for

ACPD
15, 28037–28068, 2015

(blue) January, (green) April, (yellow) July, and (red) October. The altitude of the kink at around 355 K suggests that the influence of tropical convective motion almost ceases at this level and the diabatic forcing gradually shifts to radiative heating in the TTL and above.

The diagnostic features depicted in Fig. 2 agree that the bottom of the TTL would be most properly defined at 355 K potential temperature level for our study. In the following analysis, we make use of TST trajectories defined by the air parcels that have ascended from the lower troposphere below 340 K isentrope experiencing the LCP in the TTL, which is defined by the layer between the isentropic levels 355 and 400 K within 30° N and S from the equator.

3 Results

3.1 The drop in $[H_2O]_e$

The evolution of the entry value of water to the stratosphere as modeled in $[H_2O]_e$ time series is shown in Fig. 3. The top panel is the sequential change in the monthly ensemble mean value of $[H_2O]_e$ estimated from the TST air parcels during the period between January 1997 and December 2002. We can see the decrease of the seasonal maxima in boreal summer in 2000. The seasonal minima in boreal winter, on the other hand, show larger values in January–February 2000 as compared to those in 1999, 2001, and 2002 and thus the drop in $[H_2O]_e$ is not quite obvious. As the six-year time series is not long enough to define climatology and anomalies from it, we simply view the interannual variations on the basis of each calendar month. The bottom panel of Fig. 3 is the same as the top except that the data points are connected by each calendar month. When viewed in this way, the drop in the year 2000 of about 1 ppmv shows up in the time change in September (marked by 9), October (10), November (11), and December (12). Similar drop continues to January (1) and the successive months in 2001. As there is little difference between those in August 1999 and 2000, we may

ACPD
15, 28037–28068, 2015

well conclude that the drop in $[H_2O]_e$ occurred in September 2000. Considering the time period required for the air parcels to make excursion in the TTL, we may interpret that the change in the characteristics of dehydration has been initiated in the boreal summer of 2000. The maxima of $[H_2O]_e$ in January through June 1998 are related to the strong El Niño as is discussed later in Sect. 4.

3.2 Horizontal projection of the TST trajectories

As the first step of examining the change in the characteristics of TTL dehydration initiated in northern summer of 2000, Fig. 4 illustrates the horizontal projection of TST trajectories within the layer between the isentropes 360 and 370 K extracted from those initialized in September 1999 (top) and 2000 (bottom). In spite of the equatorially symmetric assignment of the initialization points on 400 K potential temperature surface, the trajectories in the TTL are highly asymmetric with respect to the equator and clustered mostly in the northern subtropics. The dense population of the trajectories shows that the air parcels are largely trapped by Tibetan high in the region between 30° W to 150° E and 0 to 45° N. Comparison between the two, representing September trajectories prior and posterior to the drop, respectively, reveals that the circulation of air parcels around the Tibetan high is loosely tied to the center in the latter period, resulting in the expansion of the anticyclonic circulation branch mostly to the east accompanied by the spread-out of the trajectories farther to the Southern Hemisphere in the latter. This modal shift in the trajectories initialized in September occurs in the year 2000 and continues at least through 2001 and 2002 (not shown).

3.3 Statistical distribution of the LCP

The shift in the circulation pattern of air parcels is not enough to characterize the modification of dehydration efficiency in the TTL. Randel and Jensen (2013) discuss the monsoon circulation during boreal summer in the context of the influence of northern midlatitude on the TTL. The horizontal structure of ozone and water vapor on 390 K

ACPD
15, 28037–28068, 2015

potential temperature surface (Randel and Jensen, 2013, Figs. 2 and 4) suggests an intrusion of the ozone-rich midlatitude air into the TTL possibly contributing to the TTL hydration during boreal summer. For the purpose of identifying the change in the dehydration efficiency associated with the modal shift seen in Fig. 4, the numbers of LCPs are counted by every 10° longitude-latitude bin in the tropics. The probabilities of LCPs are estimated for each bin by dividing the LCP counts by the total number of TST trajectories. The top two panels of Fig. 5 show the horizontal distributions of the probabilities of LCP events thus obtained for those trajectories initialized in September 1998 and 1999 (top; prior to the drop) and September 2000, 2001 and 2002 (second panel; posterior to the drop). The spatial maximum during the period prior to the drop is found over the Bay of Bengal and Malay Peninsula with the ridge extending to South China Sea (top). During the period posterior to the drop (second panel), this maximum shows eastward expansion as far as 150° E. There also appears some increase in the Central Pacific covering both northern and southern subtropics crossing over the equator. These two components appear clearer in the difference field shown in the third panel. Those bins shown in blue (red) indicate the decrease (increase) of the LCP probabilities in the posterior period. The test statistic of the difference transformed to the standard Gaussian distribution is shown in the bottom panel of the figure indicating the region in which the differences are statistically significant at the significance level of 1 % or higher. It is interesting to note that, in addition to the dipole structure associated with the eastward expansion of the Tibetan anticyclone, the probabilities show significant decrease over the equator at around 130 to 140° E and increase in wider area almost symmetric with respect to the equator (160° E to 160° W and 10° S to 10° N). This structure will be discussed further in Sect. 4.

3.4 Statistical change in the SMR_{min}

The increase of the LCP events in some bins does not necessarily mean enhanced dehydration over there. The next step is to examine the change in the SMR_{min}. Simultaneous with counting the LCP events, the values of SMR at the time of each LCP

ACPD
15, 28037–28068, 2015

event (SMR_{min}) have been summed-up to calculate the average for each bin. Figure 6 is the same as Fig. 5 except that the ensemble mean SMR_{min} are illustrated rather than the probability of LCP events. We can see that the averages of SMR_{min} in the tropics are roughly smaller in the eastern than in the western hemisphere accompanying a broad minimum of about 3.5 to 3.7 ppmv over the maritime continent during the period prior to the drop (top). The values show general decrease in the tropics with some enhanced drop in the central Pacific reaching less than 3.0 ppmv in the period posterior to the drop (second panel from the top), leading to a reversal of zonal gradient of SMR_{min} over the equator. The difference between the two (third panel), together with the statistical significance (bottom), confirms the pronounced decrease of SMR_{min} in the central Pacific after 2000. On the other hand, the change of SMR_{min} associated with the east-west dipole structure is not so remarkable in terms of the difference of SMR_{min}, although the tendency is the same.

3.5 Statistical change in the expectation values

While the differences of SMR_{min} appear smaller over the Bay of Bengal and Malay Peninsula than over the central Pacific, the comparisons based only on the changes in SMR_{min} could be misleading, because the probabilities of LCP events are much higher in the former than in the latter (Fig. 5). Figure 7 shows the horizontal distribution of the expectation value of $[H_2O]_e$ estimated by multiplying the probability of LCP events (Fig. 5) and the ensemble mean SMR_{min} (Fig. 6) together for each bin. This corresponds to the projection of $[H_2O]_e$ onto each bin. We can see that the September values of $[H_2O]_e$ are mostly projected to the Bay of Bengal and Malay Peninsula before the drop (top panel). The contribution from this core area remains dominant during the posterior period (middle panel). The reductions (bottom panel) are mainly due to the decreases of the LCP-event probability (Fig. 5) cooperated by the reduced ensemble mean SMR_{min} (Fig. 6). The corresponding increase of LCP-event probabilities especially that over the central Pacific has contributed to a slight increase in $[H_2O]_e$ because the magnitude of increase in occurrence frequency prevails that of the de-

ACPD
15, 28037–28068, 2015

crease in SMR_{min}. The resultant changes could be interpreted as the composite of two components: (i) the decrease over the Bay of Bengal and (ii) the decrease over the equatorial western Pacific and the increase over the central Pacific almost symmetric with respect to the equator extending to the subtropical latitudes of both hemispheres. The former is supplemented by slight decrease widespread along the 10° N zonal belt with the exception around 150° E and the central Pacific. These features will be related to the eastward expansion of the anticyclonic circulation around the Tibetan high, while the latter is suggestive of some response to the thermal forcing from the equatorial ocean.

4 Discussion

4.1 Maxima of $[H_2O]_e$ in 1998

We have seen in Fig. 3 that the time series of $[H_2O]_e$ shows maxima in January through June 1998. We excluded these months from our analysis in Sect. 3 because of the influences of strong El Niño. The values of $[H_2O]_e$ in November and December 1997 are larger than those in 1998, which may suggest possible influence of El Niño also in these months. The reason why we regard these facts as little related to the drop of $[H_2O]_e$ in 2000 is briefly discussed here.

For exploration of the reason of such anomalies, the horizontal distributions of LCP are shown for those initialized in February 1997, 1998 and 1999 in Fig. 8. The distributions in February 2000, 2001 and 2002 (not shown) are similar to those of 1997 and 1999. The LCPs in February are commonly distributed almost symmetric with respect to the equator, but the longitudinal distribution is not uniform. High concentration in the western tropical Pacific in 1997 and 1999 (and also in 2000, 2001 and 2002) is suggestive of the strong influence of the warm sea surface temperature (SST) on the LCP distribution. The large scatter extending to the eastern tropical Pacific in 1998 is due to the migration of the large scale convective system to the east associated

ACPD
15, 28037–28068, 2015

with the strong El Niño. We have put this anomalous change out of the scope of the present study, because those anomalous values seem to have recovered to normal by the northern summer of 1998 (well before 2000) and there is no reasoning that this strong El Niño is coupled to the drop in $[H_2O]_e$ in 2000. For the objective judgement of the influence of the El Niño, we employ the SST averaged in the region between 90° W and 150° W longitude and 5° S to 5° N latitude (Niño 3 region, Trenberth, 1997). Those months exhibiting the SST anomalies (relative to the 1981-to-2010 climatology) greater than 1.5 times the standard deviation are excluded from the present analysis. Those excluded are the twelve months from June 1997 to May 1998.

4.2 Perspective to the mechanism of the drop

The entry value of water to the stratosphere, $[H_2O]_e$, estimated by the ensemble mean values of SMR_{min} along the TST trajectories shows appreciable decrease in September 2000 (Fig. 3), suggesting some modulation in the dehydration efficiency functioning on the air parcels advected in the TTL during the northern summer of 2000. The horizontal projection of trajectories initialized in September, characterized by anticyclonic circulation associated with Tibetan high in the TTL, shows eastward expansion in the year 2000 accompanied by some bifurcation to the Southern Hemisphere (Fig. 4). This modal shift appears as decreases in the probability distribution of the LCP over the Bay of Bengal and the western tropical Pacific (Fig. 5). The SMR averaged on the occasion of LCP events (SMR_{min}) shows general decrease with some enhancement in the central Pacific (Fig. 6). These results suggest two possible components contributing to the sudden drop of $[H_2O]_e$ in September 2000: the modulations of the Tibetan high and the thermal forcing from the equatorial ocean. The contribution from these two components has been quantified by projecting the $[H_2O]_e$ onto bins distributed in the tropics (Fig. 7). The results indicate that the drop is brought about by a response of the TTL circulation to the modulated forcing both from the continental summer monsoon and the equatorial ocean. It is thus quite interesting to take a brief look at the changes in the TTL meteorological fields in Eulerian framework before concluding this study.

ACPD
15, 28037–28068, 2015

Figure 9 illustrates the longitude-latitude section of 100 hPa geopotential height (left) and temperature (right) averaged in August 1998 and 1999 (top) and 2000, 2001 and 2002 (middle). These are the background Eulerian fields having roughly brought about the Lagrangian features described by the top two panels of Figs. 5–7. The corresponding features appear basically the same if we look at individual August without taking the average. We can see the Tibetan anticyclone in the height field of both periods (left) with the intensity weaker in the latter (2000/2001/2002). The expansion of the trajectories after 2000 (Fig. 4), therefore, is the result of loosened grip of air parcels around weakened Tibetan high in the latter years. These features remain the same in September of other years posterior to the drop (not shown). The temperature field (right-hand side) both prior and posterior to the drop appears as the typical pattern of the TTL response to the thermal forcing at the bottom boundary with additional heating to the subtropical Northern Hemisphere (Matsuno, 1966; Gill, 1980). The difference (bottom panel) indicates substantial cooling in the northern subtropics at around 150° E and the central Pacific. The latter corresponds to the findings of Rosenlof and Reid (2008) in which the tropical tropopause temperature in 171 to 200° E longitude band decreased in association with the SWV drop in 2000.

The correspondence of the decrease of the equatorial 100 hPa temperature to the increase of the underlying SST is explored in Fig. 10, which shows the longitude-time section of the equatorial SST averaged between 10° N and S of the equator. We could see the warm SST region in the western Pacific expands to the east in the year 2000, and the contour of 28 °C, the threshold of active convection (Gadgil et al., 1984), during the coldest month of the year crossed the date line in 2001. The difference between the longitudes of warm SST core and the temperature minimum near the tropopause, noticed already by Rosenlof and Reid (2008), is due to the eastward tilt of cold region associated with a steady Kelvin wave response to underlying convective heating (Hatsushika and Yamazaki, 2003). The warm condition in the central Pacific continues at least till the end of 2005. The decrease of 100 hPa temperature over the central Pacific is, thus, well correlated to this SST variation. The important point in our analysis is that

ACPD
15, 28037–28068, 2015

the drop of $[H_2O]_e$ does not come from the decrease of TTL temperature in the central Pacific but that from the water transport by way of the Bay of Bengal and the western tropical Pacific (Fig. 7).

The study by Young et al. (2012), discussing the changes in the Brewer–Dobson circulation during the period 1979 to 2005 by referring to the out-of-phase temperature relationship between the tropics and the extratropics, found no appreciable change around the year 2000. However, the zonally uniform component exhibiting the out-of-phase relationship between the tropics and the extratropics in 100 hPa temperature difference (Fig. 9) is suggestive of some stratospheric contribution to the drop in $[H_2O]_e$ (Randel et al., 2006) through wave-driven pumping (Holton et al., 1995). Actually the analysis of dynamical fields such as eddy heat flux and EP-flux by Fueglistaler (2012) finds a strengthening of the residual circulation qualitatively consistent with the drop of SWV in *October* 2000. Figure 11 shows in color the time-height section of monthly mean vertical wind velocity in the tropics. The seasonal enhancement in the upward motion during northern winter shows up in the lowermost stratosphere. The solid and dashed contours superposed on the vertical velocity field are the zonal wind components depicting the westerly and the easterly phase, respectively, of the quasi-biennial oscillation (QBO). The stagnation of the downward propagation specifically that of the easterly phase of the QBO is noticed in late 1997 to early 1998 and late 2000 to early 2001 at around 40 hPa level. This phase dependency of the stagnant propagation is brought about by the secondary circulation of the QBO in which the upward (downward) motion accompanies the easterly (westerly) shear zone of the QBO (Plumb and Bell, 1982; Hasebe, 1994). What is interesting here is that the enhanced upward motion is found in September and October 2000 blocking the downward propagation of easterlies. The limitation from our use of Eulerian vertical velocity, rather than TEM residual velocity, will be minimal as we focus our discussion in the tropics. Actually the anomalies in the equatorial upwelling at 78 hPa estimated by Rosenlof and Reid (2008) show similar results. Further analysis by Fueglistaler et al. (2014) emphasize that the strengthening of the residual circulation does not last long but continues for a few years

ACPD
15, 28037–28068, 2015

around the year 2000. Remembering the time of excursion for air parcels circulating the Tibetan high (Fig. 4), the stratospheric anomalies in October 2000 (Fueglistaler, 2012) appears later than the initiation of the drop in $[H_2O]_e$. The difference of one month, albeit small, is large enough to be resolved in the analysis. Then the enhanced upwelling discussed by Fueglistaler et al. (2014) might be the stratospheric response to the tropospheric forcing that modulated the dehydration efficiency in the preceding boreal summer of 2000 rather than the direct cause of the SWV drop. Further studies employing numerical simulations are definitely required. It is worth mentioning here that the enhancement of the Brewer–Dobson circulation may have occurred also in the northern hemispheric branch; the age of northern midlatitude stratospheric air diagnosed by the CO_2 concentration appears shorter than usual in 2002 (Engel et al., 2009, Fig. 3), although the difference is not statistically significant.

4.3 Perspective to the mechanism of sustained low amount of $[H_2O]_e$

We have seen some background meteorological fields from Eulerian perspective to interpret the evidences presumably responsible for the drop of $[H_2O]_e$ in September 2000 described in Lagrangian framework. The problems not yet answered are what is the specific event (if any) and how is it generated that has triggered the sequence of phenomena that ultimately led to the sudden drop of SWV. In addition, the sustained low values of $[H_2O]_e$ after September 2000 need some mechanism that lasts longer than the seasonal time scale, since the modulation of Tibetan high cannot explain the reduction continuing to the successive months in northern winter (Fig. 3).

Figure 12 is the same as Fig. 7 except that the January projection is illustrated. We can see, in addition to the values generally lower than those in September, the larger values are found in the western tropical Pacific (top and middle panels), indicating the January values of $[H_2O]_e$ are controlled by those over the western Pacific. This is consistent with the picture having been presented in numerical simulations (Hatsushika and Yamazaki, 2003). The difference between the two periods (the bottom diagram) shows decrease over Indonesia and increase over the central Pacific during the period

ACPD
15, 28037–28068, 2015

posterior to the drop. This pattern in January is brought about by the combination of the decrease (increase) of LCP-probability and the slight (enhanced) decrease of SMR_{min} values over the western (central) Pacific (not shown). These evidences suggest that the drop of $[H_2O]_e$ in northern winter is due to the response of the TTL circulation to the eastward expansion of the warm water to the central Pacific (Fig. 10).

The correspondence to the change in the SST distribution, the time of occurrence, and the persistency of phenomenon suggest that the drop and the subsequent low values of $[H_2O]_e$ are brought about by the eastward expansion of warm SST region to the central Pacific through reduced water entry to the stratosphere. Then our hypothetical story may read, the eastward expansion of warm SST region brings about the reduction of $[H_2O]_e$ by TST air parcels passing through the western tropical Pacific during northern winter (Fig. 12), while the heating from the modulated SST mentioned above, competing against that over the continent, has led to the modal shift of trajectories during northern summer resulting in the reduced water transport over the Bay of Bengal and the western tropical Pacific (Fig. 7).

The above speculation might end up with some proper explanation on the cause of the eastward expansion of the equatorial warm water to the central Pacific observed in 2000. In this context, it is interesting to see possible occurrence of "El Niño Modoki" characterized by the warm SST event over the central Pacific (W. J. Randel, personal communication, 2015). Actually the time series of normalized ENSO Modoki index of Ashok et al. (2007) turns from prolonged negative to positive towards 2001. It is also interesting to note that the "La Niña-like condition," tied to the surface cooling of the equatorial eastern Pacific, is supposedly responsible for the recent hiatus, the pause of the global-mean surface air temperature rise through the strengthening of ocean heat uptake (Kosaka and Xie, 2013; Watanabe et al., 2014). If proved to be true, we may have unveiled another piece of pathways the internal variability of our climate system could exert on the surface cooling through SST-driven SWV fluctuations.

ACPD
15, 28037–28068, 2015

5 Conclusions

Backward kinematic trajectories, initialized on 400 K potential temperature surface in the tropics, have been employed to describe the stratospheric water drop observed at around 2000 to 2001 from a Lagrangian point of view. The entry value of water to the stratosphere, $[H_2O]_e$, shows appreciable decrease in the trajectories initialized in September 2000 suggesting the change in the TTL dehydration efficiency during the boreal summer of 2000. The following changes are found to be responsible for the drop in $[H_2O]_e$. The reduction of water vapor transported by those air parcels that experienced LCP events in two regions; over the Bay of Bengal and the western tropical Pacific. The reductions are brought about by the decreases in both the LCP-event probability and the ensemble mean SMR_{min} over there. The LCP reduction in the former region is related to the modified migration pathways of air parcels circulating the weakened Tibetan anticyclone, while that in the latter may be a response to eastward expansion of warm water to the central Pacific. This SST modulation seems to be responsible also for the decrease of $[H_2O]_e$ in the successive northern winter. Some indication of stratospheric contribution through intensified pumping appears only intermittent and will be better interpreted as a response to tropospheric forcing changes.

Acknowledgements. This work is based on the Master of Science Thesis of T. Noguchi submitted to the Graduate School of Environmental Science, Hokkaido University in February 2015. T. Noguchi is grateful to the members of the Graduate School of Environmental Science for the encouragement and discussions through the preparation of his thesis. The discussion with Koji Yamazaki of Hokkaido University is greatly appreciated. The results in part have been presented at the CT3LS Meeting having been held in July 2015. F. Hasebe is grateful to the comments from meeting participants especially W. J. Randel of NCAR and K. H. Rosenlof of NOAA. NOAA OI SST V2 data are provided by the NOAA/OAR/ESRL PSD, Boulder, Colorado, USA, from their Web site at http://www.esrl.noaa.gov/psd/. This work was supported by the Japan Society for the Promotion of Science, Grant-in-Aid for Scientific Research (S) 26220101.

ACPD
15, 28037–28068, 2015

References

Ashok, K., Behera, S. K., Rao, S. A., Weng, H., and Yamagata, T.: El Niño modoki and its possible teleconnection, J. Geophys. Res., 112, c11007, doi:10.1029/2006JC003798, 2007. 28052

Bönisch, H., Engel, A., Birner, Th., Hoor, P., Tarasick, D. W., and Ray, E. A.: On the structural changes in the Brewer–Dobson circulation after 2000, Atmos. Chem. Phys., 11, 3937–3948, doi:10.5194/acp-11-3937-2011, 2011. 28039

Dee, D. P., Uppala, S. M., Simmons, A. J., Berrisford, P., Poli, P., Kobayashi, S., Andrae, U., Balmaseda, M. A., Balsamo, G., Bauer, P., Bechtold, P., Beljaars, A. C. M., van de Berg, L., Bidlot, J., Bormann, N., Delsol, C., Dragani, R., Fuentes, M., Geer, A. J., Haimberger, L., Healy, S. B., Hersbach, H., Hólm, E. V., Isaksen, L., Kållberg, P., Köhler, M., Matricardi, M., McNally, A. P., Monge-Sanz, B. M., Morcrette, J. J., Park, B. K., Peubey, C., de Rosnay, P., Tavolato, C., Thépaut, J. N., and Vitart, F.: The ERA-interim reanalysis: configuration and performance of the data assimilation system, Q. J. Roy. Meteor. Soc., 137, 553–597, 2011. 28041

Dessler, A. E., Schoeberl, M. R., Wang, T., Davis, S. M., Rosenlof, K. H., and Vernier, J.-P.: Variations of stratospheric water vapor over the past three decades, J. Geophys. Res.-Atmos., 119, 12588–12598, doi:10.1002/2014JD021712, 2014. 28039

Engel, A., Möbius, T., Bönisch, H., Schmidt, U., Heinz, R., Levin, I., Atlas, E., Aoki, S., Nakazawa, T., Sugawara, S., Moore, F., Hurst, D., Elkins, J., Schauffler, S., Andrews, A., and Boering, K.: Age of stratospheric air unchanged within uncertainties over the past 30 Years, Nat. Geosci., 2, 28–31, 2009. 28051

Fueglistaler, S.: Stepwise changes in stratospheric water vapor?, J. Geophys. Res., 117, D13302, doi:10.1029/2012JD017582, 2012. 28039, 28050, 28051

Fueglistaler, S., Bonazzola, M., Haynes, P. H., and Peter, T.: Stratospheric water vapor predicted from the Lagrangian temperature history of air entering the stratosphere in the tropics, J. Geophys. Res., 110, D08107, doi:10.1029/2004JD005516, 2005. 28039, 28040, 28041

Fueglistaler, S., Abalos, M., Flannaghan, T. J., Lin, P., and Randel, W. J.: Variability and trends in dynamical forcing of tropical lower stratospheric temperatures, Atmos. Chem. Phys., 14, 13439–13453, doi:10.5194/acp-14-13439-2014, 2014. 28039, 28050, 28051

Fujiwara, M., Vömel, H., Hasebe, F., Shiotani, M., Ogino, S.-Y., Iwasaki, S., Nishi, N., Shibata, T., Shimizu, K., Nishimoto, E., Canossa, J. M. V., Selkirk, H. B., and Oltmans, S. J.:

ACPD
15, 28037–28068, 2015

Seasonal to decadal variations of water vapor in the tropical lower stratosphere observed with balloon-borne cryogenic frostpoint hygrometers, J. Geophys. Res., 115, D18304, doi:10.1029/2010JD014179, 2010. 28039
Gadgil, S., Joseph, P. V., and Joshi, N. V.: Ocean-atmosphere coupling over monsoon regions, Nature, 312, 141–143, 1984. 28049
Gill, A. E.: Some simple solutions for heat-induced tropical circulation, Q. J. Roy. Meteor. Soc, 106, 447–462, 1980. 28049
Hasebe, F.: Quasi-biennial oscillations of ozone and diabatic circulation in the equatorial stratosphere, J. Atmos. Sci., 51, 729–745, 1994. 28050
Hatsushika, H. and Yamazaki, K.: Stratospheric drain over Indonesia and dehydration within the tropical tropopause layer diagnosed by air parcel trajectories, J. Geophys. Res., 108, 4610, doi:10.1029/2002JD002986, 2003. 28039, 28049, 28051
Hegglin, M. I., Plummer, D. A., Shepherd, T. G., Scinocca, J. F., Anderson, J., Froidevaux, L., Funke, B., Hurst, D., Rozanov, A., Urban, J., von Clarmann, T., Walker, K. A., Wang, H. J., Tegtmeier, S., and Weigel, K.: Vertical structure of stratospheric water vapour trends derived from merged satellite data, Nat. Geosci., 7, 768–776, doi:10.1038/ngeo2236, 2014. 28039
Holton, J. R. and Gettelman, A.: Horizontal transport and the dehydration of the stratosphere, Geophys. Res. Lett., 28, 2799–2802, 2001. 28039
Holton, J. R., Haynes, P. H., McIntyre, M. E., Douglass, A. R., Rood, R. B., and Pfister, L.: Stratosphere-troposphere exchange, Rev. Geophys., 33, 403–439, 1995. 28042, 28050
Kosaka, Y. and Xie, S.-P.: Recent global-warming hiatus tied to equatorial Pacific surface cooling, Nature, 501, 403–407, 2013. 28052
Matsuno, T.: Quasi-geostrophic motions in the equatorial area, J. Meteorol. Soc. Jpn., 44, 25–43, 1966. 28049
Oltmans, S. J. and Hofmann, D. J.: Increase in lower-stratospheric water vapour at a mid-latitude Northern Hemisphere site from 1981 to 1994, Nature, 374, 146–149, 1995. 28039
Oltmans, S. J., Vömel, H., Hofmann, D. J., Rosenlof, K. H., and Kley, D.: The increase in stratospheric water vapor from balloonborne, frostpoint hygrometer measurements at Washington, D.C., and Boulder, Colorado, Geophys. Res. Lett., 27, 3453–3456, 2000. 28039
Plumb, R. A. and Bell, R. C.: A model of the quasi-biennial oscillation on an equatorial beta-plane, Q. J. Roy. Meteor. Soc., 108, 335–352, 1982. 28050

ACPD
15, 28037–28068, 2015

Randel, W. J. and Jensen, E. J.: Physical processes in the tropical tropopause layer and their roles in a changing climate, Nat. Geosci., 6, 169–176, doi:10.1038/NGEO1733, 2013. 28044, 28045

Randel, W. J., Wu, F., Vömel, H., Nedoluha, G. E., and Forster, P.: Decreases in stratospheric water vapor after 2001: links to changes in the tropical tropopause and the Brewer–Dobson circulation, J. Geophys. Res., 111, D12312, doi:10.1029/2005JD006744, 2006. 28039, 28050

Rosenlof, K. H. and Reid, G. C.: Trends in the temperature and water vapor content of the tropical lower stratosphere: sea surface connection, J. Geophys. Res., 113, D06107, doi:10.1029/2007JD009109, 2008. 28039, 28049, 28050

Scherer, M., Vömel, H., Fueglistaler, S., Oltmans, S. J., and Staehelin, J.: Trends and variability of midlatitude stratospheric water vapour deduced from the re-evaluated Boulder balloon series and HALOE, Atmos. Chem. Phys., 8, 1391–1402, doi:10.5194/acp-8-1391-2008, 2008. 28039

Shindell, D. T.: Climate and ozone response to increased stratospheric water vapor, Geophys. Res. Lett., 28, 1551–1554, 2001. 28039

Solomon, S., Rosenlof, K. H., Portmann, R. W., Daniel, J. S., Davis, S. M., Sanford, T. J., and Plattner, G.-K.: Contributions of stratospheric water vapor to decadal changes in the rate of global warming, Science, 327, 1219–1223, 2010. 28039

Trenberth, K. E.: The definition of El Niño, B. Am. Meteorol. Soc., 78, 2771–2777, 1997. 28048

Watanabe, M., Shiogama, H., Tatebe, H., Hayashi, M., Ishii, M., and Kimoto, M.: Contribution of natural decadal variability to global warming acceleration and hiatus, Nature Clim. Change, 4, 893–897, doi:10.1038/Nclimate2355, 2014. 28052

Young, P. J., Rosenlof, K. H., Solomon, S., Sherwood, S. C., Fu, Q., and Lamarque, J.-F.: Changes in stratospheric temperatures and their implications for changes in the Brewer–Dobson circulation, 1979–2005, J. Climate, 25, 1759–1772, doi:10.1175/2011JCLI4048.1, 2012. 28050

ACPD
15, 28037–28068, 2015

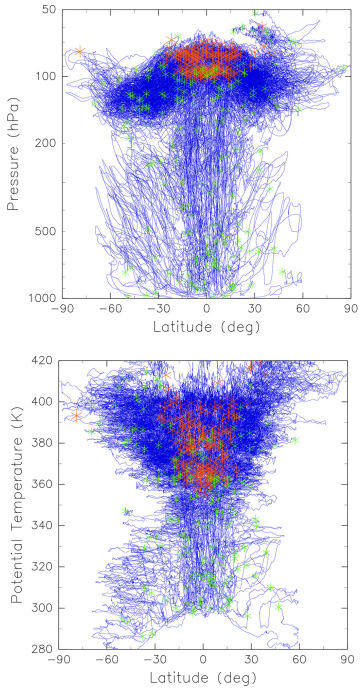

Figure 1. The meridional projections in (top) pressure and (bottom) isentropic coordinates of 90 day kinematic backward trajectories initialized on 400 K potential temperature surface at 15 January 1999. Initial positions are set at 5.0° longitude by 1.5° latitude gridpoints covering the tropical zone within 30° N and S from the equator. Those shown here are the subsets in which the initial positions are trimmed to 20.0° by 6.0° gridpoints for visual clarity. The asterisks marked in red are the Lagrangian Cold Points, while those in green are the termination points of trajectory calculations. The calculations end up if the backward extension of the trajectories hit the surface of the earth even in less than 90 days before initialization.

ACPD
15, 28037–28068, 2015

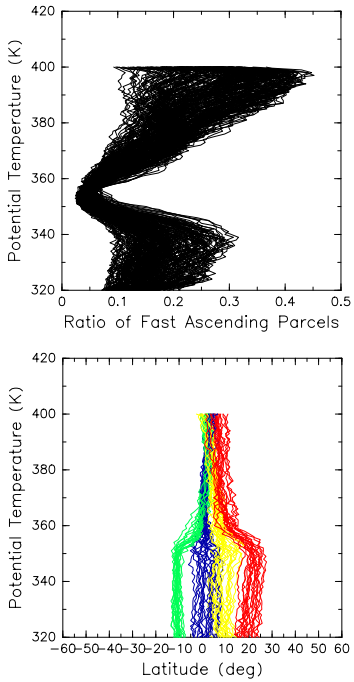

Figure 2. The vertical profiles of (top) proportion of the "fast" ascending air parcels and (bottom) averaged ascending track diagnosed by 90 day kinematic back trajectories that extends from 400 K to the lower troposphere below 340 K potential temperature surface. The upward motion on θ K isentrope is categorized as "fast" if the air parcel crosses θ K surface from below $\theta - 0.1$ K to above $\theta + 0.1$ K in 30 min. Each line in the top panel shows the daily proportion of trajectories at each isentropic level that correspond to "fast" ascending air parcels. The ascending tracks in the bottom panel are color-coded on a monthly basis (January in blue, April in green, July in yellow, and October in red) to visualize the seasonal migration of the ascending latitude in the tropics.

ACPD
15, 28037–28068, 2015

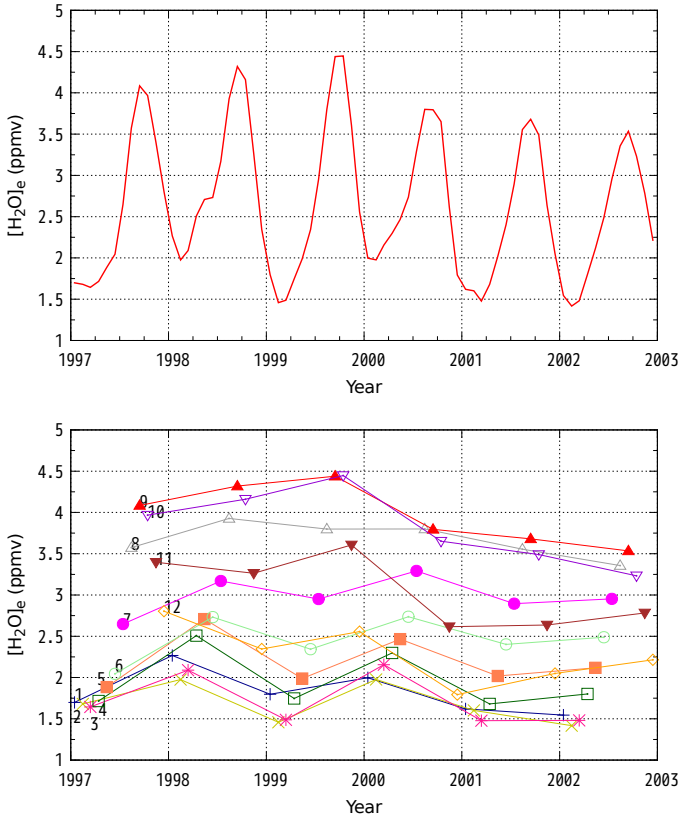

Figure 3. The time series of the ensemble mean values of $[H_2O]_e$ (ppmv) estimated from the TST trajectories initialized on the corresponding month. The data points are connected by sequential month on the top panel, while they are linked by each calendar month to visualize interannual variations on a monthly basis in the bottom. The labels 1 through 12 designate January through December of each year. The significance interval at 1 % level is roughly the size of each symbol in the lower panel.

ACPD
15, 28037–28068, 2015

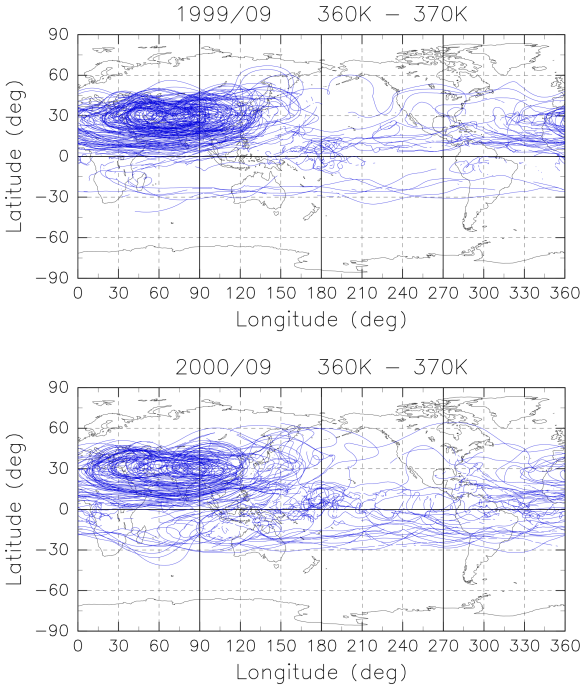

Figure 4. Horizontal projection of the backward trajectories extracted within the potential temperature levels between 360 and 370 K. The initialization is made on 400 K potential temperature surface between 30° N and S from the equator (Sect. 2) in (top) September 1999 and (bottom) September 2000. The illustration is limited to the subset of trajectories as in Fig. 1 for visual clarity.

ACPD
15, 28037–28068, 2015

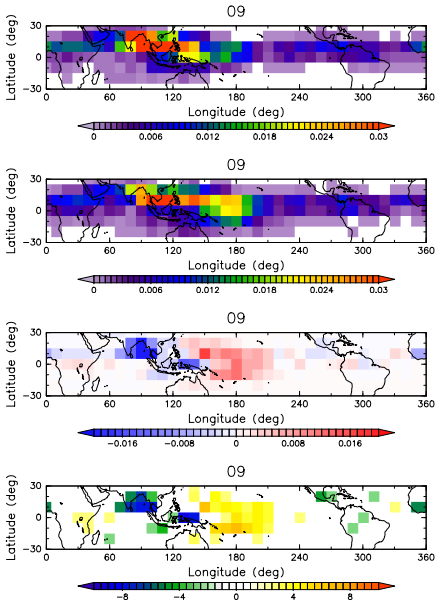

Figure 5. Horizontal distribution of LCP-event probability estimated from the TST trajectories initialized on 400 K in (top) September 1998 and 1999 (prior to the drop) and (second from the top) September 2000, 2001 and 2002 (posterior to the drop). The probabilities are estimated in 10° by 10° longitude–latitude bin as the number of LCPs experienced by all TST air parcels inside the bin divided by the total number of TST parcels used for the calculation. The difference of probabilities between the two (posterior minus prior to the drop) and the values of test statistic transformed to the standard Gaussian distribution are shown in the third and the bottom panel, respectively. The test statistic is derived from the difference of the ratio of LCP occurrences assuming binomial distribution for the two populations. The colored bins indicate that the difference is statistically significant at the significance level of 1 % or higher. Those bins shown in white indicate there found no LCP event in the top two panels, while the difference is not statistically significant in the bottom two.

ACPD
15, 28037–28068, 2015

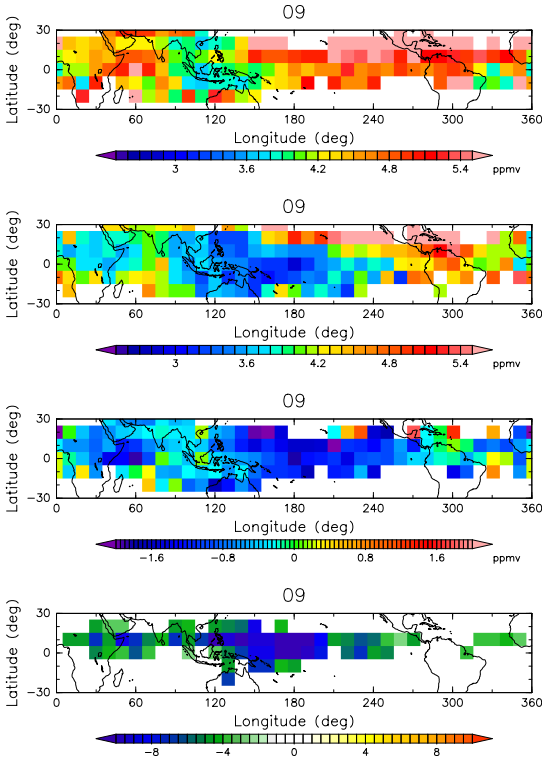

Figure 6. The same as Fig. 5 except that the ensemble mean values of SMR_{min} are illustrated on the bin-by-bin basis. The test statistic is *t* values derived from the difference of sample means.

ACPD
15, 28037–28068, 2015

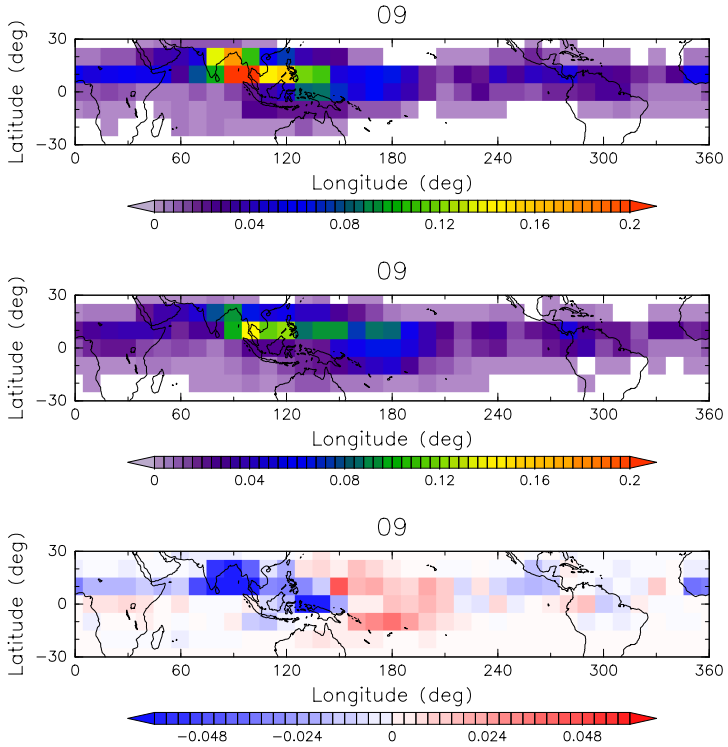

Figure 7. The same as the top three panels of Fig. 6 except that the contribution of each bin to the $[H_2O]_e$ (ppmv) is illustrated. The value for each bin is the expectation value as calculated by multiplying the probability (Fig. 5) by the ensemble mean SMR_{min} (Fig. 6).

ACPD
15, 28037–28068, 2015

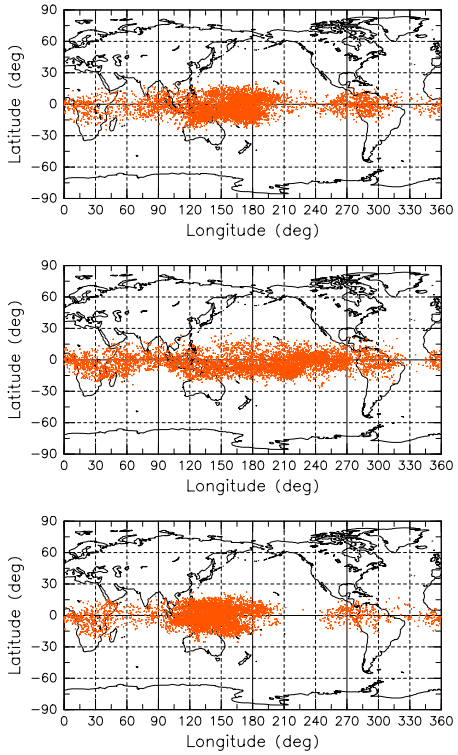

Figure 8. Horizontal distribution of LCP taken by all TST trajectories initialized on 400 K isentrope in February (top) 1997, (middle) 1998, and (bottom) 1999.

ACPD
15, 28037–28068, 2015

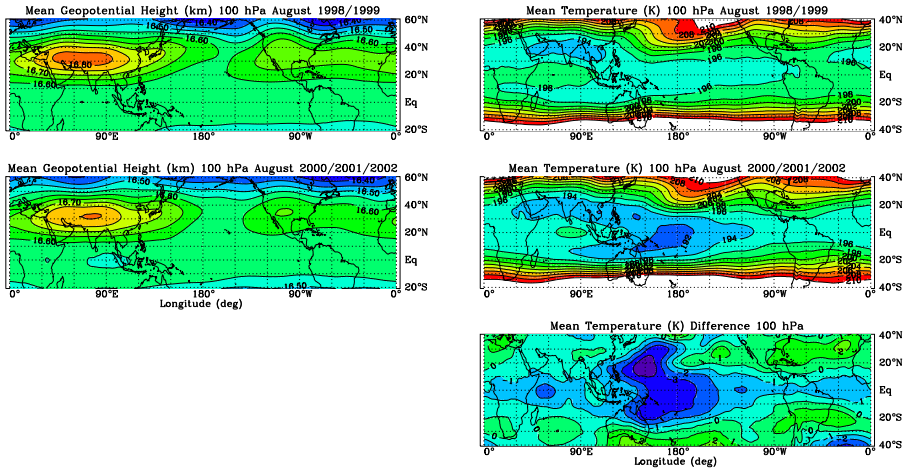

Figure 9. Longitude-latitude sections of (left) geopotential height (km) and (right) temperature (K) on 100 hPa averaged in August 1998 and 1999 (top) and 2000, 2001 and 2002 (middle) and the difference between the two (bottom) estimated from ERA Interim dataset. Note the difference of latitudinal range between the left and the right side figures.

ACPD
15, 28037–28068, 2015

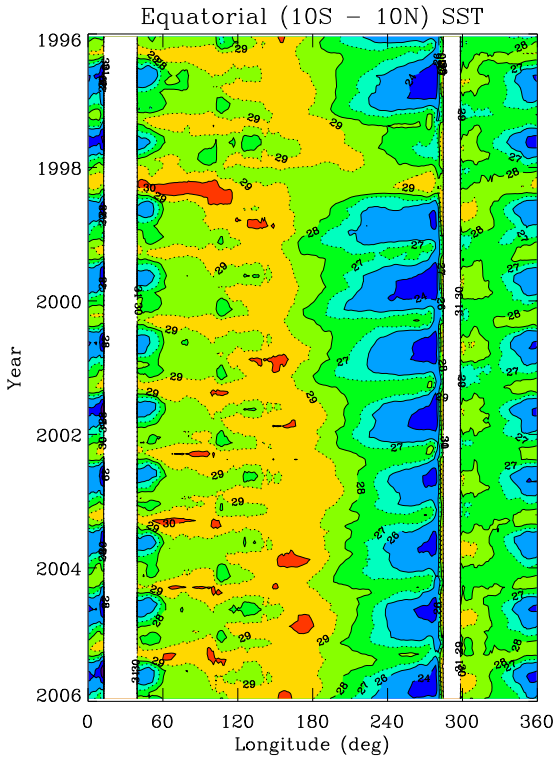

Figure 10. Longitude-time section of sea surface temperature (SST) averaged over the oceanic region of the latitude band between 10° N and S of the equator during the period from January 1996 to December 2005. Data are from NOAA OI SST V2.

ACPD
15, 28037–28068, 2015

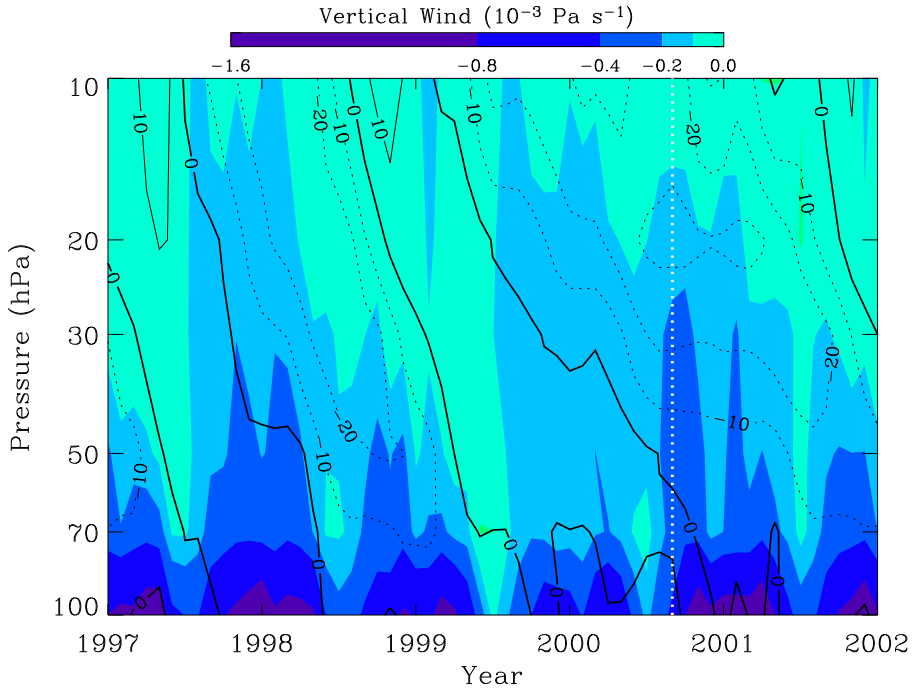

Figure 11. Time-height section of the zonally and latitudinally (within 15° N and S) averaged monthly mean vertical (color; 10^{-3} Pa s^{-1}) and zonal (contour; m s^{-1}) wind velocities from January 1997 to December 2001 calculated from ERA Interim dataset. Solid (dashed) contours are westerlies (easterlies). Tick marks are January of the corresponding year, and the vertical dashed line in white marks September 2000.

ACPD
15, 28037–28068, 2015

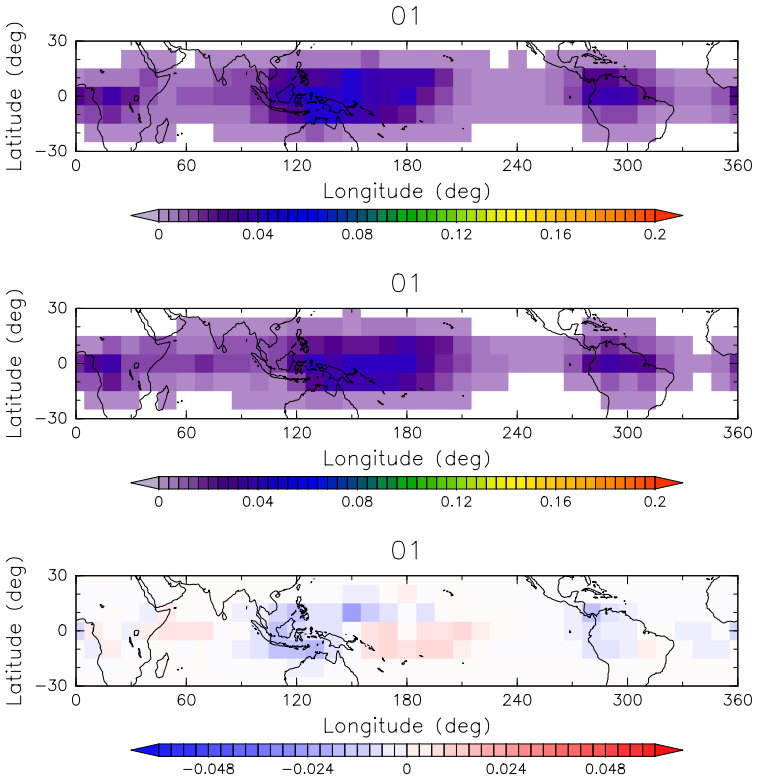

Figure 12. The same as Fig. 7 but for January. Those values in 1997, 1999, and 2000 are used for the calculations prior to the drop, while 2001 and 2002 are used for the posterior. Those in January 1998 are not used due to the influence of El Niño (see text).

ACPD
15, 28037–28068, 2015